JACS
JOURNAL OF THE AMERICAN CHEMICAL SOCIETY
Article
pubs.acs.org/JACS

Three-Way Crystal-to-Crystal Reversible Transformation and Controlled Spin Switching by a Nonporous Molecular Material

José Sánchez Costa,*[,‡] Santiago Rodríguez-Jiménez,[‡] Gavin A. Craig,[‡] Benjamin Barth,[‡] Christine M. Beavers,[§] Simon J. Teat,[§] and Guillem Aromí*[,‡]

[‡]Departament de Química Inorgànica, Universitat de Barcelona, Diagonal, 645, 08028 Barcelona, Spain
[§]Advanced Light Source, Berkeley Laboratory, 1 Cyclotron Road, Berkeley, California 94720, United States

Supporting Information

ABSTRACT: Porous materials capable of hosting external molecules are paramount in basic and applied research. Nonporous materials able to incorporate molecules via internal lattice reorganization are however extremely rare since their structural integrity usually does not resist the guest exchange processes. The novel heteroleptic low-spin Fe(II) complex $[Fe(bpp)(H_2L)](ClO_4)_2{\cdot}1.5C_3H_6O$ (**1**; bpp = 2,6-bis(pyrazol-3-yl)pyridine, H_2L = 2,6-bis(5-(2-methoxyphenyl)pyrazol-3-yl)pyridine) crystallizes as a compact discrete, nonporous material hosting solvate molecules of acetone. The system is able to extrude one-third of these molecules to lead to $[Fe(bpp)(H_2L)](ClO_4)_2{\cdot}C_3H_6O$ (**2**), switching to the high-spin state while experiencing a profound crystallographic change. Compound **2** can be reversed to the original material upon reabsorption of acetone. Single crystal X-ray diffraction experiments on the latter system (**1′**) and on **2** show that these are reversible single-crystal-to-single-crystal (SCSC) transformations. Likewise, complex **2** can replace acetone by MeOH and H_2O to form $[Fe(bpp)(H_2L)](ClO_4)_2{\cdot}1.25MeOH{\cdot}0.5H_2O$ (**3**) through a SCSC process that also implies a switch to the spin state. The **3**→**1** transformation through acetone reabsorption is also demonstrated. Besides the spin switching at room temperature, this series of SCSC transformations causes macroscopic changes in color that can be followed by the naked eye. The reversible exchanges of chemicals are therefore easily sensed at the temperature at which these occur, contrary to what is the case for most of the few existing nonporous spin-based sensors, which feature a large temperature gap between the process monitored and the mechanism of detection.

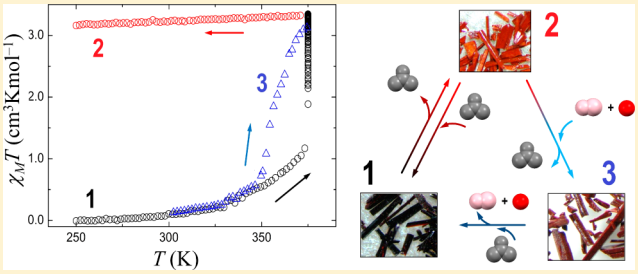

INTRODUCTION

The development of chemical sensors capable of detecting small volatile organic compounds and toxic gases by simple means is a critical task for environmental and energy science.[1] A principle for the design of chemosensors is that they must be able to detect substances and produce an easily measurable response, such as a change of color, of fluorescence, or of any other macroscopic property.[2] One approach to achieve this kind of material is through the construction of porous coordination polymers (PCPs)[3] (or metal organic frameworks, MOFs),[4] which by their nature contain the voids necessary to absorb guest molecules, thereby changing their properties.[5] In the absence of pores, such exchange might still take place through a process of diffusion throughout the crystal lattice.[6−8] These phenomena are, however, extremely rare in crystalline molecular materials[9] since the absence of long-range covalent interactions usually leads to the collapse of the lattice. In some of the documented examples, the exchangeable solvents can directly coordinate to the metal center,[10−12] causing significant changes to the d−d absorptions. Otherwise, the guests intercalate within the crystal lattice, influencing the supramolecular interactions within the material. Ideally, in the latter case the metal center may be sensitive to subtle changes thus resulting in alterations to some physical properties. Good candidates for exploiting these effects are spin crossover (SCO) complexes.[13] In fact, SCO complexes present the ability to switch between high-spin (HS) and low-spin (LS) electronic states in response to external stimuli, such as temperature or pressure variations, light irradiation, or the inclusion of analytes. In particular, some systems are known to be very sensitive to solvent exchange through the molecular network.[14] The transition implies distinctly different magnetic, optical, electrical, and structural outputs.[15] Thus, in a limited number of PCPs,[16] mainly the Hoffmann Clathrate-type systems, indirect analyte−metal interactions can be enough to afford a spin-state change of Fe(II) centers. On the other hand, to the best of our knowledge there is only one well characterized Fe(II) discrete molecular material system that shows vapochromism as a result of SCO, while maintaining the integrity of its crystal lattice.[17,18]

We have been engaged in the design of new molecular SCO materials through the synthesis and use of derivatives of the ligand 2,6-bis-(pyrazol-3-yl)pyridine (bpp, Figure 1),[19] as we

Received: November 19, 2013
Published: February 20, 2014

   dx.doi.org/10.1021/ja411595y | J. Am. Chem. Soc. 2014, 136, 3869−3874

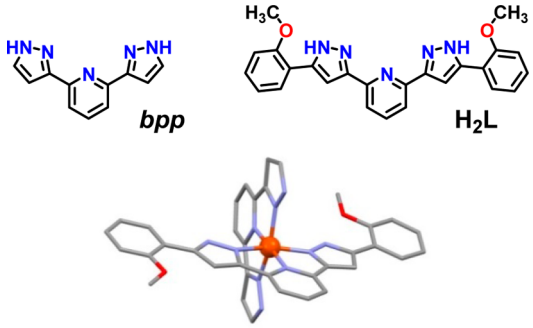

Figure 1. Ligands bpp and H_2L (top) and representation of the cation $[Fe(bpp)(H_2L)]^{2+}$ of **1**. Orange, Fe; red, O; purple, N; gray, C. Hydrogen atoms not shown.

have recently reported.[20−22] The ligand bpp gives rise to a family of coordination complexes, many exhibiting SCO, with general formula $[Fe(bpp)_2]A{\cdot}xH_2O$ (A = anions), which often are extremely sensitive to their degree of hydration.[23] For example, the LS, trihydrated phase of the triflate salt becomes a SCO system upon desorption of two molecules of water, displaying a huge hysteresis loop (up to 140 K wide).[24] The tetrafluoroborate derivative of a $[Fe(Me\text{-}bpp)_2)]^{2+}$ cation (Me-bpp, a methyl-substituted bpp) exhibits up to five different crystallographic phases with varying degrees of hydration and SCO responses.[25] The rationalization of the exact influence of water in the spin active species in this and other related systems is however hampered by the lack of structural information on the pertinent individual phases.[26]

Attaching hydroxyphenyl moieties at the ends of bpp enhances the intermolecular interactions within the lattice of the corresponding Fe(II) complexes, yielding a variety of responses as a function of the solvent of crystallization present.[20−22] We were thus intrigued by the possibility of combining these properties with the capabilities for exchanging guest molecules demonstrated by complexes of simpler bpp. With this in mind, we prepared a novel bpp-based ligand, 2,6-bis(5-(2-methoxyphenyl)pyrazol-3-yl)pyridine (H_2L, Figure 1), and combining it with bpp, we managed to produce the heteroleptic coordination complex $[Fe(bpp)(H_2L)](ClO_4)_2{\cdot}1.5C_3H_6O$ (**1**). This compound has turned out to exhibit a remarkable three-way single-crystal-to-single-crystal (SCSC) transformation process involving the reversible exchange of small volatile molecules at room temperature. These transformations are coupled to dramatic optical, magnetic, and crystallographic changes, thus converting this nonporous material into a robust room-temperature switch, sensitive to methanol and acetone.

RESULTS AND DISCUSSION

Description of $[Fe(bpp)(H_2L)](ClO_4)_2{\cdot}1.5C_3H_6O$ (**1**). Dark-red single crystals of **1** were obtained from the reaction of bpp, H_2L, and $Fe(ClO_4)_2$ in acetone. The complex crystallizes in the monoclinic space group $P2_1/n$ (Table 1), with an asymmetric unit comprising one $[Fe(bpp)(H_2L)]^{2+}$ cation (Figure 1), together with two perchlorate anions and a total of 1.5 molecules of acetone (Figure S1). Both bpp-type ligands coordinate the metal in a mer fashion through their three N-donor atoms, providing the metal with a distorted octahedral geometry. The ligand H_2L is in a syn,anti configuration of the methoxyphenyl rings with respect to the central coordination pocket. The average Fe−N bond length at 250 K is 1.949 Å

Table 1. Crystallographic Data of 1−3

	1	2	3
T (K)	250	250	100
cryst. system	monoclinic	triclinic	triclinic
space group	$P2_1/n$	$P\text{-}1$	$P\text{-}1$
a (Å)	14.0569(17)	13.099(5)	12.708(4)
b (Å)	21.606(3)	13.355(5)	13.214(5)
c (Å)	15.2698(19)	14.078(5)	14.931(5)
α (°)	90	71.968(4)	71.792 (4)
β (°)	114.946	69.923(4)	69.208 (4)
γ (°)	90	70.857(4)	62.660 (4)
V (Å^3)	4205.0(9)	2130.8(2)	2048.2(12)
Oct. volume (Å^3)	9.515	12.474	9.507
$R1$ (all data)	0.0512	0.1055	0.0781
$wR2$ (all)	0.1372	0.3050	0.2357
av. Fe−N (Å)	1.949	2.169	1.947
solv. accessible voids (Å^3)	0	34	0

(Table S1), indicating that the Fe(II) centers are in the LS state.[22]

The complexes of **1** organize in sheets according to the so-called terpyridine embrace,[27] where each cation interacts with its four first neighbors via $\pi\cdots\pi$ contacts reinforced by C−H$\cdots\pi$ interactions (Figure S2). The differing dimensions of both ligands allow interactions with second neighbors that otherwise would not be possible. This is believed to be one of the driving forces leading to the heteroleptic compound over any of the two possible homoleptic species (not observed). The sheets are then connected to each other through additional $\pi\cdots\pi$ contacts, together with hydrogen-bonding motifs involving the ClO_4^- groups and the N−H groups of the cations (Figure S1 and Table S2 and S3). The solvents of crystallization are located in between the sheets. Of these, the full molecule of acetone is well ordered, forming an H-bond with the N−H moiety of bpp, whereas the molecule with half occupancy is disordered over two positions and only loosely bound. It must be noted that the lattice exhibits no significant pores or channels (Figure S3).

Conversion between 1 and $[Fe(bpp)(H_2L)](ClO_4)_2{\cdot}C_3H_6O$ (2). To test for the desorption of acetone and the potential consequent physical changes, a single crystal of **1** was heated to 375 K and kept at this temperature for 2 h under a dry N_2 flow. During the course of this process, the crystal changed color from dark-red to orange, while maintaining its structural integrity. After cooling to 250 K, a single crystal X-ray diffraction experiment was performed to determine the structure. The new system was found now in the triclinic $P\text{-}1$ space group. The change of space groups was accompanied by a 50% reduction of the cell volume and the disappearance of the disordered molecules of acetone. The new material thus exhibits the composition $[Fe(bpp)(H_2L)](ClO_4)_2{\cdot}C_3H_6O$ (**2**, Figure S4). Other remarkable transformations unveiled by the new structure are the simultaneous rotation by ∼180° of both methoxyphenyl groups of H_2L in every other cation (thus maintaining the syn,anti arrangement, Figure 2) together with a change to the average Fe−N bond distances, to 2.169 Å, which are the values expected for Fe(II) centers in the HS state[22] (Table S4 and Figure S4). The new compound exhibits an analogous network of intermolecular interactions as its precursor, while presenting a nonporous character (Figure S5 and Table 1). Thus, a drastic crystallographic phase transition, together with a dramatic change in optical properties (see SI) and spin state, has occurred after the desorption of acetone

dx.doi.org/10.1021/ja411595y | J. Am. Chem. Soc. 2014, 136, 3869−3874

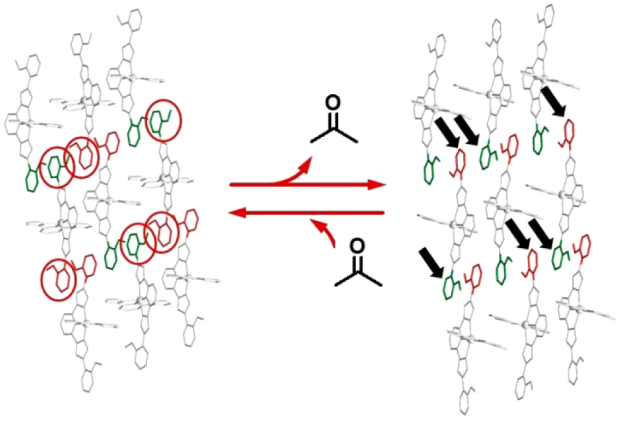

Figure 2. Representation of the SCSC reversible transformation between **1** and **2**, emphasizing the ~180° rotation of the methoxyphenyl groups from every other complex (only the $[Fe(bpp)(H_2L)]^{2+}$ cations are represented).

(one-half molecule per complex cation) in a process that must occur by diffusion through the nonporous lattice, in a manner that permits the persistence of the crystallographic order throughout the bulk of the single crystal (Figure 3). This process was monitored by optical reflectivity (Figure S6) and optical microscopy on a single crystal (see SI, movie 1).

Compound **2** could be obtained intact also by heating **1** for 2h in an oven at 390 K, as determined also by single crystal X-ray diffraction. The reversibility of the process was demonstrated by exposing single crystals of **2** to a room-temperature saturated atmosphere of acetone for 24 h. After the exposure, the dark-red color was recovered, while the quality of the resulting crystals allowed a new X-ray diffraction determination. The crystal structure (**1′**) was found to be virtually identical to that of the initial phase **1** (Tables 1, S1 and S2), thus confirming that upon reabsorption of acetone, the entire crystallographic transition previously demonstrated together with all the changes in physicochemical properties could be reversed entirely without causing damage to the crystal lattice. This reversible process was monitored on single crystals by optical reflectivity (Figure S7) and optical microscopy (SI, movie 2) and in the bulk by thermogravimetric analysis (TGA) experiments and magnetometric measurements (see below and SI).

Absorption/Desorption of [MeOH + H_2O] Involving $[Fe(bpp)(H_2L)](ClO_4)_2·1.25MeOH·0.5H_2O$ (3). The capacity of **2** to incorporate acetone vapors into the structure concomitant to drastic changes in properties stimulated attempts to detect in a similar manner other small volatile molecules, such as MeOH. Thus, exposure of **2** to saturated vapors of MeOH at room temperature for 24 h caused the recovery of a dark-red color with persistence of the crystallinity. A single crystal X-ray diffraction study of this material was possible and revealed a new formulation for the novel system, $[Fe(bpp)(H_2L)](ClO_4)_2·1.25MeOH·0.5H_2O$ (**3**), as a result of the complete exchange[28] of the acetone molecules by methanol and atmospheric water (Figure S8). This process does not lead to a change in space group, which remains as triclinic *P*-1, while the unit cell volume is approximately maintained (Table 1). The Fe(II) cations are organized in the lattice as with the acetone precursor (Figure S9), now with the methanol molecules playing an analogous role; one forms a hydrogen bond with one N−H group from bpp, while the other one, with 25% occupancy, is disordered over two positions and loosely bound. In addition, a molecule of water with 50% occupancy forms an H-bond with the ordered MeOH molecule and with a ClO_4^- group (Figure S8). Quite remarkably, the average Fe−N bond distance at 100 K is now 1.947 Å, which means that the replacement of acetone by MeOH and H_2O also causes a change in magnetic state to LS (Table S7, see below). As with the acetone solvates, there are no pores inside the crystal lattice (see Table 1 and SI). This process could also be monitored through optical reflectivity experiments (Figure S7) and was

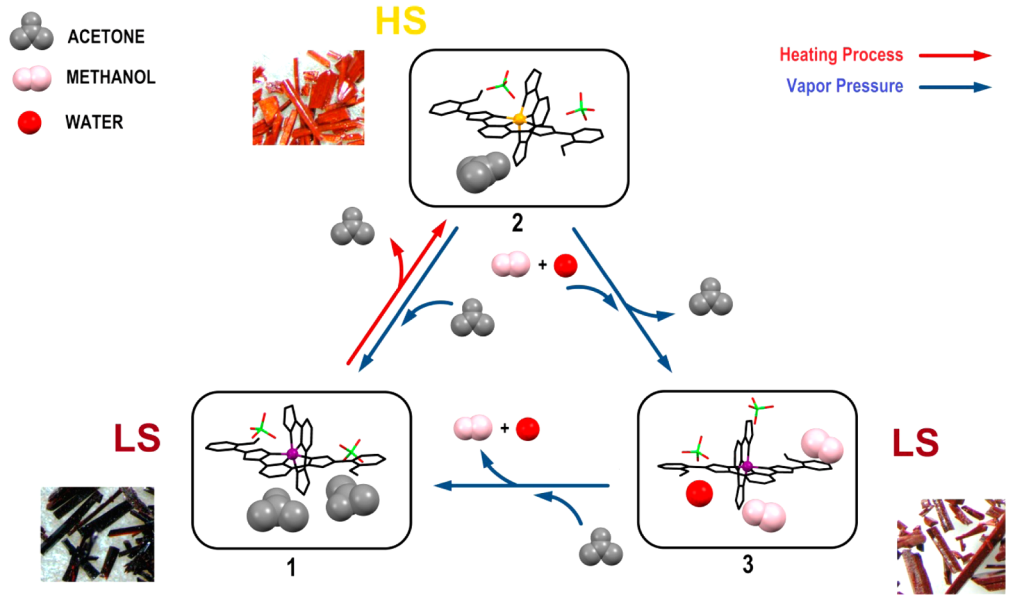

Figure 3. Representation of the molecular structure of **1**−**3** (only major component of disordered species shown) emphasizing the full conversion cycle undergone by these three species through subsequent absorption, desorption, or exchange of small molecules. Among the represented processes are the three-way proven crystal-to-crystal transformations discussed in the text (see SI). Pictures of the corresponding single crystals are also shown.

dx.doi.org/10.1021/ja411595y | *J. Am. Chem. Soc.* 2014, 136, 3869−3874

recorded on a single crystal by optical microscopy experiments (SI, movie 3).

The effect of the vapors of acetone on the hydromethanolated material **3** was also studied. Thus, exposure of these crystals to a saturated atmosphere of acetone at room temperature for 24h caused the replacement of the methanol and water molecules again by acetone molecules to return to the original compound **1** (Figure 3). The identity of this material was consistent with microanalysis, TGA analysis, and magnetic studies (see below and SI). These experiments show that the lattice of $[Fe(bpp)(H_2L)](ClO_4)_2$ solvated with acetone not only reversibly evacuates acetone but also can be cycled through a process of desorption of acetone, absorption of methanol and water, followed by full replacement of these solvents by acetone (Figure 3) back to the original compound. The cycle could be achieved with the same crystals more than once as proved again by TGA and magnetic measurements (see below and SI).

Magnetic Switching Behavior. The changes in spin state observed for the various transformations described above provide this material with potential as a spin-based sensor. This was further investigated through variable-temperature magnetic susceptibility measurements. Thus the bulk magnetization of a polycrystalline sample of **1** was measured in the 2−375 K temperature range under a constant magnetic field of 0.5 T. The $\chi_M T$ vs T curve (χ_M is the molar paramagnetic susceptibility, Figure 4, top) shows that the compound is diamagnetic (LS) until nearly 300 K, consistent with the observations from single crystal X-ray diffraction. From that temperature, the $\chi_M T$ product starts to increase slightly as a result of a gradual change of Fe(II) from LS to HS. When the temperature reached 375 K, the heating was stopped, while the $\chi_M T$ product continued to rise. After 2 h at this temperature, the magnetic response reached a saturation value close to 3.25 cm^3 K mol^{-1}, which is slightly above the figure expected (3.00 cm^3 K mol^{-1}) for Fe(II) ions with an $S = 2$ spin state (HS) and $g = 2$. On cooling down the sample back to 2 K (Figure S10), the $\chi_M T$ value remains practically constant down to near 240 K, where it experiences an abrupt decrease to a value of 0.3 cm^3 K mol^{-1}. This is consistent with a process of SCO with $T_{1/2\downarrow}$ of 235 K. After bringing the system to 6 K, the temperature was raised again to 300 K. At 236 K the product $\chi_M T$ increases fast up to a value of 2.8 cm^3 K mol^{-1} at 265 K, corresponding to Fe(II) in the HS state ($T_{1/2\uparrow}$ = 240 K). Compound **2** is thus a SCO system featuring a small hysteresis loop 5 K wide. The X-ray diffraction experiments of **2** at 250 K indeed confirm it to be in the HS state. The reversibility of the process could also be monitored by optical reflectivity, which was conducted over at least three full cycles (Figure S11).

A sample of **2** exposed to saturated acetone at room temperature for 24 h was measured in the magnetometer in the same conditions as above proving that it became diamagnetic again, consistent with the process of reabsorption of acetone to reform **1**, as unveiled by single crystal X-ray crystallography. These observations represent a direct proof of the spin switching processes accompanying the absorption or desorption of acetone molecules by lattices of $[Fe(bpp)(H_2L)](ClO_4)_2$. The reversibility and robustness of the process could be monitored by measuring the magnetic response after successive steps of absorption and desorption of acetone (Figure S12), and it was verified by measuring the TGA of each recovered phase of **1** (Figure S13). The absorption of methanol by **2** was also monitored through magnetic measurements.

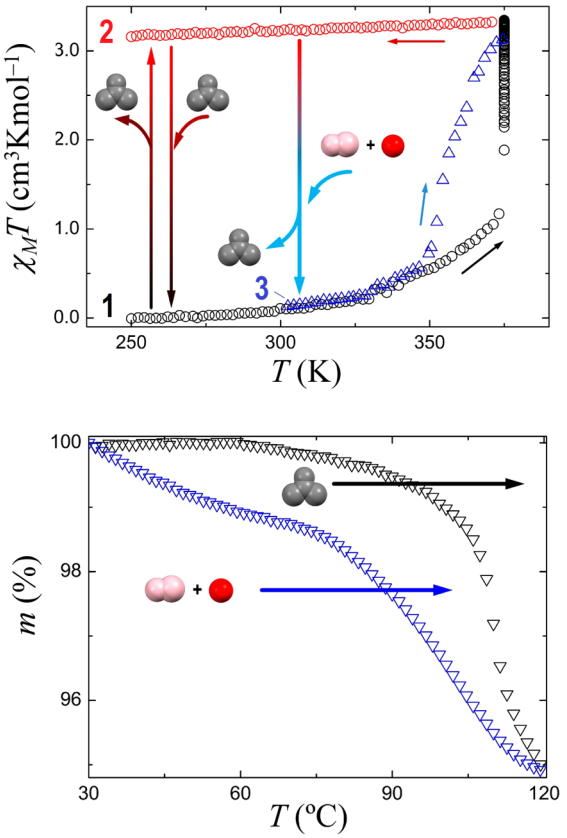

Figure 4. (top) Plots of $\chi_M T$ vs T for **1** upon warming and concomitant desorption of acetone (black circles), for resulting compound **2** upon cooling (red circles) and for **3** (blue triangles, formed from **2**, after substitution of acetone by MeOH + H_2O) upon warming from room temperature and concomitant depletion of MeOH + H_2O. The crystal-to-crystal transformations described in the text (**1**→**2**, **2**→**1**, and **2**→**3**) are shown with vertical arrows positioned, for clarity, at arbitrary temperatures. (bottom) TGA graphs for the desorption of acetone (from **1**, black symbols) and MeOH + H_2O (from **2**, blue symbols), emphasizing the difference in temperatures for these two processes, consistent with the observations from magnetic measurements.

Thus a polycrystalline sample of this system exposed to methanol vapors as described above was measured through variable-temperature magnetization at 0.5 T, from 300 to 375 K.

The $\chi_M T$ vs T curve (Figure 4, top) confirms the fact that the compound **3** is diamagnetic. Upon warming, the value of $\chi_M T$ slowly increases until the temperature reaches 350 K, where the rise of magnetic response becomes more abrupt, attaining a value of 3.00 cm^3 K mol^{-1} at 375 K. This shows that the system progressively changes from LS to HS until the transition becomes complete at the highest measured temperature. This process seems analogous to that observed for **1** and is also due to a process of desolvation. After this process takes place, the compound exhibits a different magnetic behavior (Figure S14). In fact, if the temperature of 375 K is maintained, the $\chi_M T$ product gradually diminishes down to an equilibrium value of 1.9 cm^3 K mol^{-1}, which corresponds to having approximately two-thirds of the spin centers in the HS state. This is either the result of a process of relaxation from a metastable state to an equilibrium situation or the final step of a complete solvent depletion. Upon cooling from the equilibrium, the $\chi_M T$ value decreases to vanish almost completely near 200 K, in a process

dx.doi.org/10.1021/ja411595y | J. Am. Chem. Soc. 2014, 136, 3869−3874

that corresponds to a SCO. On warming again, the $\chi_M T$ vs T curve superimposes with the cooling branch up to 375 K (and not with the curve originally seen for **3**), which is consistent with a process of SCO of the system in equilibrium (Figure S14).

TGA experiments comparing the behavior of **1** and **3** suggest that indeed both systems experience the expected solvent loss following the increase in temperature; 0.5 mol of acetone in one case and to 1 mol of MeOH plus 1 mol of water in the other (Figures S15 and S16). The difference in desorption temperatures (Figure 4, bottom) are in agreement with the effects observed through magnetometry. This difference was maintained when cycling the system between the three different structurally characterized phases more than once.

The system depleted of MeOH/H_2O by heating, remained crystalline, however, it could not be characterized by single crystal X-ray diffraction. Nevertheless, it was exposed to saturated methanol vapors for 24 h. The magnetic measurement of the resulting system recreated the behavior seen for **3** (Figure 4, top), suggesting that the hydro-methanolated product was regenerated and that this process of solvent depletion and reabsorption was also reversible. This was corroborated through TGA measurements (Figure S17) by repeating the transformation over two cycles. The fact that both solvent systems studied (acetone and MeOH/H_2O, respectively) exhibit a distinctly different temperature of desorption provides a fingerprint that enhances the interest of investigating in the future the response of this lattice to other analytes.

Like the replacement of MeOH and H_2O by acetone in the transformation of **3** into **1** (Figures 2, S18 and S19), the formation of **1**, as obtained from heating **3** and exposing it to acetone vapors, was also corroborated by EA, TGA and magnetometry (Figures S20 and S21).

■ CONCLUSIONS AND OUTLOOK

In summary, the lattice of the heteroleptic molecular coordination complex $[Fe(bpp)(H_2L)](ClO_4)_2$ has proven to exhibit remarkable small-molecule exchange abilities accompanied by drastic variations on the structure and physicochemical properties. Surprisingly, the observed processes of desorption/absorption or exchange are fully reversible with persistence of the crystallinity, despite the fact that the lattice is nonporous and nonpolymeric. This is the result of a subtle balance between flexibility of end moieties of H_2L in **1**, combined with a robust network of intermolecular interactions. This opens up perspectives for developing this and related compounds as potential sensors of small molecules in the gas phase, by exploiting the robustness of the system and the possibility of following this process through a variety of common techniques. We are currently investigating these promising avenues by exploring the absorption and exchange of a large variety of other analytes.

■ EXPERIMENTAL SECTION

Synthesis of the Organic Ligands. Ligand 2,6-bis(pyrazol-3-yl)pyridine (bpp) was synthesized as described in the literature.[29]

2,6-bis(3-oxo-3-(2-methoxyphenyl)-propionyl)pyridine (H_2L1). 2-Methoxyacetophenone (5.44 g, 36.2 mmol) and ethyl-2,6-pyridinedicarboxylate (4.04 g, 18.1 mmol) were dissolved in dimethoxyethane (DME, 200 mL) under a nitrogen atmosphere. A 60% oil dispersion of NaH (8.35 g, 208.8 mmol) was washed for 20 min under N_2 with hexane. The solvent was extracted using a filter cannula, and DME (50 mL) was added. This suspension was added dropwise with stirring to the above mixture. After the addition was completed, the reaction mixture was heated to reflux, turning from yellow to orange after a few hours, and left overnight. The mixture was then left to cool to room temperature, and some drops of EtOH were added in order to quench any remaining NaH, followed by careful addition of 100 mL of water. Acetic acid (20 mL) was then added, which led to a change of color to orange and a change of texture while a precipitate formed. After adding about 75% of the acetic acid, the mixture turned suddenly dark brown, and the precipitate dissolved. The resulting two layers were separated and the organic phase was extracted with diethyl ether. The combined organic phases were dried over $MgSO_4$, and the solvent removed in vacuum. The product is a yellow solid. The yield was 3.91 g (50%). ^{1}H NMR (400 MHz, ppm in $CDCl_3$): 16.3 (s, 2H), 8.3 (d, 2H), 8.06 (t, 1H), 7.96 (dd, 2H), 7.72 (s, 2H), 7.48 (td, 2H), 7.06 (dd, 2H), 6.95 (dt, 2H), 3.8 (s, 6H). IR (KBr pellet)/cm^{-1}: 3432 w, 2923 w, 2847 w, 1600 s, 1489 s, 1464 m, 1284 m, 1243 s, 1180 m, 1020 w, 992 m, 814 m, 763 m, 615 m. Mass $(M + H)^+$ 432.2. EA, calcd (%) for $C_{25}H_{21}NO_6$ (found): C, 69.6 (69.15); H, 4.91 (4.91); N, 3.25 (3.27).

2,6-bis(5-(2-methoxyphenyl)-pyrazol-3-yl)pyridine (H_2L). Solid H_2L1 (2 g, 4.64 mmol) was refluxed overnight with hydrazine monohydrate (0.44 g, 9.27 mmol) in MeOH (120 mL). After cooling to room temperature, the off-white suspension was filtered and washed with diethyl ether to afford a white precipitate which was dried in air. The yield was 1.72g (87%). ^{1}H NMR (400 MHz, ppm in DMSO-d_6): 13.5 (broad s, 2H), 7.98 (broad t, 1H), 7.90 (broad m, 2H), 779 (broad m, 2H), 7.36 (m, 4H), 7.14 (dd, 2H), 7.04 (m, 2H), 3.93 (s, 6H). IR (KBr pellet)/cm^{-1}: 3314 s, 3175 s, 2922 s, 1602 m, 1576 s, 1477 s, 1443 m, 1292 s, 1181 s, 1032 m, 1004 m, 958 m, 797 m, 738 s. Mass $(M + H)^+$ 424.4. EA, calcd (%) for $C_{25}H_{21}N_5O_2$ H_2O (found): C, 68.00 (67.60); H, 5.25 (5.23); N, 15.86 (15.42).

Coordination Complexes. *$[Fe(bpp)(H_2L)](ClO_4)_2 \cdot 1.5 C_3H_6O$ (**1**).* A suspension of H_2L (0.026 g, 0.06 mmol) and bpp (0.013 g, 0.06 mmol) in acetone (10 mL) was added dropwise with stirring to a solution of $Fe(ClO_4)_2 \cdot 6H_2O$ (0.034 g, 0.13 mmol) and ascorbic acid (~3 mg) in acetone (10 mL). The resulting orange solution was stirred for 45−60 min at room temperature, before being filtered and layered with diethyl-ether (volume 1:1). Crystals suitable for X-ray diffraction formed after 2 days (0.038 g, 65%). IR (KBr pellet)/cm^{-1}: 3404 (m), 3145 (w), 2942 (w), 1615 (w), 1474 (m), 1259 (w), 1121 (s), 1112 (s), 1089 (s), 1015 (m), 775 (m), 625 (m). EA, calcd (%) for $C_{36}H_{30}Cl_2FeN_{10}O_{10} \cdot 1.5C_3H_6O$ (found): C, 49.81 (49.30); H, 4.03 (4.04); N, 14.34 (14.45).

*$[Fe(bpp)(H_2L)](ClO_4)_2 \cdot C_3H_6O$ (**2**).* Crystals of compound **1** were brought to 120 °C in an oven for 2 h, inducing a color change from dark red to orange. The heating process caused the loss of 0.5 mol of acetone per formula unit. IR (KBr pellet)/cm^{-1}: 3408 (w), 2948 (w), 1615 (w), 1475 (m), 1255 (w), 1120 (s), 1108 (s), 1092 (s), 1080 (s), 1014 (m), 767 (m), 624 (m). EA, calcd (%) for $C_{36}H_{30}Cl_2FeN_{10}O_{10} \cdot 0.96C_3H_6O \cdot 0.8H_2O$ (found): C, 48.66 (48.17); H, 3.92 (3.56); N, 14.60 (15.1).

*$[Fe(bpp)(H_2L)](ClO_4)_2 \cdot 1.25CH_4O \cdot 0.5H_2O$ (**3**).* Crystals of **2** were exposed to saturated methanol vapors during 24 h. During the process the crystals changed colors from orange to dark red. IR (KBr pellet)/cm^{-1}: 3405 (w), 2928 (w), 1615 (w), 1476 (m), 1260 (w), 1122 (s), 1108 (s), 1100 (s), 1074 (s), 1014 (m), 772 (m), 623 (m). EA, calcd (%) for $C_{36}H_{30}Cl_2FeN_{10}O_{10} \cdot 1.25CH_4O \cdot H_2O$ (found): C, 47.22 (46.66); H, 3.94 (3.67); N, 14.78 (15.26).

X-ray Crystallography Data Collection. Data were collected at different temperatures for **1**−**3** and **1′** using a Bruker APEX II CCD diffractometer on station 11.3.1 of the Advanced Light Source at Lawrence Berkeley National Laboratory, at λ = 0.7749 Å, from a silicon 111 monochromator. The structures were solved by direct methods. The integration of diffraction profiles and absorption corrections were made with the SAINT[30] and SADABS[31] programs. Materials for publication were prepared using SHELXTL,[32] PLATON,[33] Mercury 1.4,[34] and Olex2[35] programs. Olex2 has been used for calculating the solvent accessible voids.

Physical Measurements. Variable-temperature magnetic susceptibility data were obtained with a Quantum Design MPMS-XL SQUID magnetometer at the "Unitat de Mesures Magnètiques" of the

dx.doi.org/10.1021/ja411595y | J. Am. Chem. Soc. 2014, 136, 3869−3874

Universitat de Barcelona. Pascal's constants were used to estimate diamagnetic corrections to the molar susceptibility, and a correction was applied for the sample holder. The optical reflectivity variation was gauged by optical microscopy, using a MOTIC SMZ-140 optical stereoscope equipped with a charge-coupled device (CCD) camera MOTICAM1000 and a white halogen lamp as a light source. Images were collected in RGB format without any filter with the mean value from each region of interest (ROI) analyzed under the ImageJ environment. The temperature was controlled by using a Linkam THMS600 liquid-nitrogen cryostat. Movies 2 and 3 were recorded at room temperature with a double vessel assembly; an external vessel containing the solvents and a small internal pot holding the sample, allowing filming the color change with the CCD camera. IR spectra were recorded on KBr pellets, in the range 4000−400 cm^{-1}, with a Thermo Nicolet Avatar 330 FT-IR spectrometer. Elemental analyses were performed with a Perkin-Elmer Series II CHNS/O Analyzer 2400 at the "Servei de Microanàlisi" of CSIC, Barcelona.

■ ASSOCIATED CONTENT

Supporting Information

The molecular characterization of the crystalline samples and the experimental details for studies of absorption−desorption behavior, including the magnetic behavior of all the species. This material is available free of charge via the Internet at http://pubs.acs.org

■ AUTHOR INFORMATION

Corresponding Authors

josesanchezcosta@gmail.com
guillem.aromi@qi.ub.es

Notes

The authors declare no competing financial interest.

■ ACKNOWLEDGMENTS

G.A. thanks the ERC for a Starting Grant (258060 FuncMolQIP). The authors thank the Spanish MCI through CTQ2009-06959 (JSC, GAC and GA) and through CTQ2012-32247 (GA). The Advanced Light Source is supported by the Director, Office of Science, Office of Basic Energy Sciences of the U.S. Department of Energy under contract no. DE-AC02-05CH11231.

■ REFERENCES

(1) *An Introduction to Indoor Air Quality (IAQ) Volatile Organic Compounds (VOCs)*; EPA: Washington, DC, 2012; http://www.epa.gov/iaq/voc.html.
(2) Wenger, O. S. *Chem. Rev.* **2013**, *113*, 3686−3733.
(3) Horike, S.; Shimomura, S.; Kitagawa, S. *Nature Chem.* **2009**, *1*, 695−704.
(4) Inokuma, Y.; Yoshioka, S.; Ariyoshi, J.; Arai, T.; Hitora, Y.; Takada, K.; Matsunaga, S.; Rissanen, K.; Fujita, M. *Nature* **2013**, *495*, 461−466.
(5) Ohba, M.; Yoneda, K.; Agusti, G.; Muñoz, M. C.; Gaspar, A. B.; Real, J. A.; Yamasaki, M.; Ando, H.; Nakao, Y.; Sakaki, S.; Kitagawa, S. *Angew. Chem., Int. Ed.* **2009**, *48*, 4767−4771.
(6) Coronado, E.; Giménez-Marqués, M.; Espallargas, G. M.; Brammer, L. *Nat. Commun.* **2012**, *3*, 828.
(7) Niel, V.; Thompson, A. L.; Muñoz, M. C.; Galet, A.; Goeta, A. E.; Real, J. A. *Angew. Chem,. Int. Ed.* **2003**, *42*, 3760−3763.
(8) Galet, A.; Muñoz, M. C.; Real, J. A. *Chem. Commun.* **2006**, 4321−4323.
(9) Huang, Z.; White, P. S.; Brookhart, M. *Nature* **2010**, *465*, 598−601.
(10) Supriya, S.; Das, S. K. *J. Am. Chem. Soc.* **2007**, *129*, 3464−3465.
(11) Albrecht, M.; Gossage, R. A.; Lutz, M.; Spek, A. L.; van Koten, G. *Chem.—Eur. J.* **2000**, *6*, 1431−1445.
(12) Albrecht, M.; Lutz, M.; Spek, A. L.; van Koten, G. *Nature* **2000**, *406*, 970−974.
(13) Bousseksou, A.; Molnár, G.; Salmon, L.; Nicolazzi, W. *Chem. Soc. Rev.* **2011**, *40*, 3313−3335.
(14) Halder, G. J.; Kepert, C. J.; Moubaraki, B.; Murray, K. S.; Cashion, J. D. *Science* **2002**, *298*, 1762−1765.
(15) Gütlich, P.; Goodwin, H. A. *Spin Crossover in Transition Metal Compounds*; Springer-Verlag: Berlin, 2004; Vol. *I*−*III*.
(16) Muñoz, M. C.; Real, J. A. *Coord. Chem. Rev.* **2011**, *255*, 2068−2093.
(17) Li, B.; Wei, R.-J.; Tao, J.; Huang, R.-B.; Zheng, L.-S.; Zheng, Z. *J. Am. Chem. Soc.* **2010**, *132*, 1558−1566.
(18) Wei, R.-J.; Tao, J.; Huang, R.-B.; Zheng, L.-S. *Inorg. Chem.* **2011**, *50*, 8553−8564.
(19) Halcrow, M. A. *Coord. Chem. Rev.* **2009**, *253*, 2493−2514.
(20) Craig, G. A.; Costa, J. S.; Roubeau, O.; Teat, S. J.; Aromí, G. *Chem.—Eur. J.* **2012**, *18*, 11703−11715.
(21) Craig, G. A.; Costa, J. S.; Roubeau, O.; Teat, S. J.; Aromí, G. *Eur. J. Inorg. Chem.* **2013**, 745−752.
(22) Craig, G. A.; Costa, J. S.; Roubeau, O.; Teat, S. J.; Aromí, G. *Chem.—Eur. J.* **2011**, *17*, 3120−3127.
(23) Marcen, S.; Lecren, L.; Capes, L.; Goodwin, H. A.; Letard, J. F. *Chem. Phys. Lett.* **2002**, *358*, 87−95.
(24) Buchen, T.; Gutlich, P.; Sugiyarto, K. H.; Goodwin, H. A. *Chem.—Eur. J.* **1996**, *2*, 1134−1138.
(25) Roberts, T. D.; Tuna, F.; Malkin, T. L.; Kilner, C. A.; Halcrow, M. A. *Chem. Sci.* **2012**, *3*, 349−354.
(26) Clemente-Leon, M.; Coronado, E.; Giménez-López, M. C.; Romero, F. M. *Inorg. Chem.* **2007**, *46*, 11266−11276.
(27) McMurtrie, J.; Dance, I. *CrystEngComm* **2005**, *7*, 230−236.
(28) Wu, C. D.; Lin, W. B. *Angew. Chem., Int. Ed.* **2005**, *44*, 1958−1961.
(29) Camparini, A.; Ponticelli, F.; Tedeschi, P. *J. Heterocycl. Chem.* **1977**, *14*, 435−438.
(30) *SAINT Plus, Data Reduction and Correction Program*, v. 6.01; Bruker AXS, Inc.: Madison, Wisconsin, 1998.
(31) *SADABS, Bruker/Siemens Area Detector Absorption Correction Program*, v.2.01; Bruker AXS, Inc.:Madison, Wisconsin, 1998.
(32) Sheldrick, G. M. *Acta Crystallogr., Sect. A* **2008**, *64*, 112−122.
(33) *PLATON, A Multipurpose Crystallographic Tool*; Utrecht University: Utrecht, The Netherlands, 2008.
(34) Macrae, C. F.; Edgington, P. R.; McCabe, P.; Pidcock, E.; Shields, G. P.; Taylor, R.; Towler, M.; van de Streek, J. *J. Appl. Crystallogr.* **2006**, *39*, 453−457.
(35) Dolomanov, O. V.; Bourhis, L. J.; Gildea, R. J.; Howard, J. A. K.; Puschmann, H. *J. Appl. Crystallogr.* **2009**, *42*, 339−341.